Structurally Pure and Reproducible Polymer Materials for High-Performance Organic Solar Cells

SMEETS, Sander; LIU, Quan; VANDERSPIKKEN, Jochen; Quill, Tyler James; GIELEN, Sam; LUTSEN, Laurence; VANDEWAL, Koen & MAES, Wouter (2023)
Structurally Pure and Reproducible Polymer Materials for High-Performance Organic Solar Cells. In: CHEMISTRY OF MATERIALS, 35 (19) , p. 8158 -8169.

DOI: 10.1021/acs.chemmater.3c01646
Handle: http://hdl.handle.net/1942/41572

Structurally pure and reproducible polymer materials for high-performance organic solar cells

Sander Smeets[a,b,c], Quan Liu[a,b,c], Jochen Vanderspikken[a,b,c], Tyler James Quill[d], Sam Gielen[a,b,c], Laurence Lutsen[a,b,c], Koen Vandewal[a,b,c], Wouter Maes[a,b,c,*]

[a] *Hasselt University, Institute for Materials Research (IMO), Agoralaan Building D, 3590 Diepenbeek, Belgium*
[b] *IMEC, Associated Lab IMOMEC, Wetenschapspark 1, 3590 Diepenbeek, Belgium*
[c] *Energyville, Thorpark, 3600 Genk, Belgium*
[d] *Stanford University, Department of Materials Science and Engineering, Stanford, CA 94305, USA*

corresponding author: wouter.maes@uhasselt.be

Abstract

The commercial uptake of organic solar cells is (amongst others) hindered by poor reproducibility of the device performance, arising from the variability in molar mass distribution and the presence of structural defects in push-pull conjugated polymers. Traditional 'in-flask' synthesis methods and commonly used catalysts contribute to these issues. Flow chemistry has been proposed to provide consistent molar masses, while a recently applied Buchwald catalyst shows promise for reduced structural defect formation. However, this catalyst has not been used for donor polymers affording state-of-the-art efficiencies in organic solar cells, such as PM6 and D18. In this work, we utilize these two polymers as model systems to probe the effect of different synthetic conditions and examine the precise chemical structures, including any homocoupled defects present, by matrix-assisted laser desorption/ionization time-of-flight (MALDI–ToF) mass spectrometry. Additionally, we analyze how these structural factors impact the material and device properties. By combining droplet-flow chemistry and defect-free synthesis, we demonstrate a reproducible and scalable protocol for the synthesis of donor polymers with a tailorable molar mass for high-efficiency organic photovoltaics.

Introduction

Donor-acceptor (also called push-pull) conjugated polymers have been a topic of considerable research interest for nearly 20 years. They are prime candidates for numerous applications such as organic photovoltaics (OPVs), photodetectors, and (electrochemical) transistors due to their tunable optoelectronic, charge transport, and solubility/miscibility properties, via rational design of the constituent donor and acceptor building blocks.[1-3] However, several hurdles remain toward large-scale commercialization of these polymers and the emerging technologies relying on said materials. One of these obstacles is the variation in quality between different polymer batches. On the one hand, batch-to-batch variations are inherent to the polycondensation approach used to prepare these push-pull conjugated polymers, inevitably leading to (small) molar mass differences. On the other hand, the observed variations are sometimes attributed to the upscaling of lab-scale 'in-flask' procedures.[4, 5] Issues with mass and heat transfer lead to differences in molar mass (distribution), which can result in an unfavorable photoactive layer blend morphology, diminished charge transport properties, and inferior performance in optoelectronic devices.[6-8] Flow chemistry can offer a solution to these problems while providing additional benefits such as easier scalability and enhanced safety.[9] In particular, droplet-flow synthesis has demonstrated excellent reproducibility, both in terms of molar mass distribution and optoelectronic properties of the synthesized conjugated polymers.[10, 11]

The intrinsic chemical structure can also play a role in causing batch-to-batch variations. Although direct arylation polymerization has certainly gained traction, the Stille polymerization, which couples an aryl distannane (usually the more electron-rich or donor) monomer with an aryl dibromide (usually the more electron-poor or acceptor) monomer with the aid of a palladium catalyst (Figure 1), remains the work-horse method to synthesize these materials.[12, 13] Treated as a reliable and orthogonal way of cross-coupling donor and acceptor monomers, little attention is given to the actual polymer structures and a perfect alternation of the constituent monomers is often implicitly assumed without further notice.

The picture of perfectly alternating conjugated polymers with only the monomer's respective end-groups is, however, far from reality.[14] Although these end-groups can survive the polymerization (depending on the reaction time), side reactions of the Stille cross-coupling, such as dehalogenation and destannylation, usually terminate the chain, thereby affording hydrogen or methyl end-groups. Furthermore, ligands from the catalytic system can also be incorporated into the final structure by ligand exchange.[15, 16] A prime example of this is the incorporation of phenyl ligands from tetrakis ($Pd(PPh_3)_4$).[17] Besides termination, side reactions can also cause homocoupling, where two donor or two acceptor moieties are coupled directly.[18, 19] Several pathways have been proposed to explain the presence of these structural defects (Figure 1).[19, 20] Homocoupling of the donor (organotin) moieties MAY arise through a Pd(II) species, either added as such or as the product of oxidizing impurities (e.g. oxygen) in the reaction medium. Similarly, a reducing impurity can convert Ar-Pd(II)-Br species to $Ar\text{-}Pd(0)^-$, which can undergo a second oxidative addition to induce acceptor homocoupling. When conducting a Stille polymerization, it is evident that high monomer purities and carefully maintained inert conditions are essential to eliminate the possibility of these side reactions to their fullest extent.[17] However, homocoupling can still be observed even when taking utmost care. Arylpalladium species are prone to disproportionation, which results in acceptor homocoupling and Pd(II), opening up the pathway to donor homocoupling. Homocoupling has been found to affect absorption, molecular packing, and charge transport properties, as well as final (solar cell) device performance.[18, 21-24] Apart from the utilized monomers, the choice of the catalyst and ligand can also have a profound impact on the amount of homocoupling.[25]

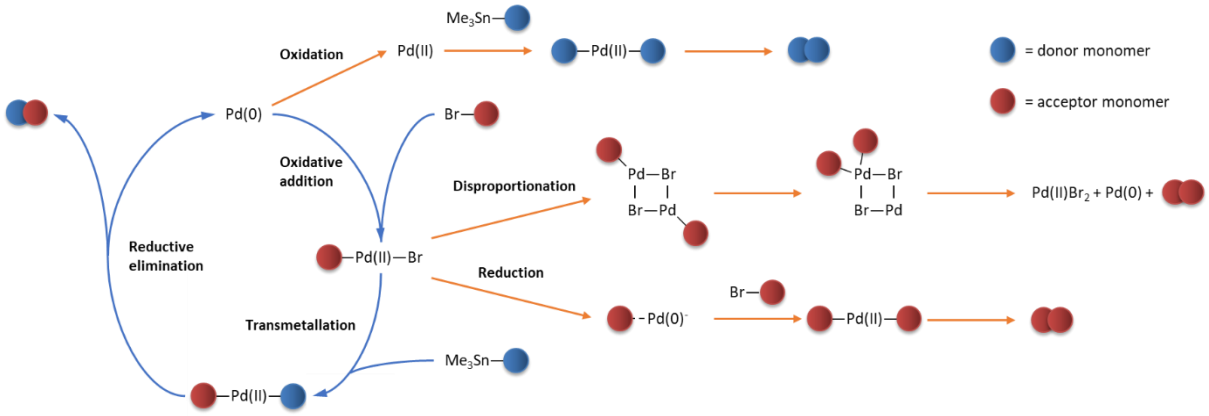

Figure 1: A simplified overview of the Stille cycle (blue) and the pathways leading to homocoupling (orange). Adapted from reference 20. Copyright 2014 John Wiley and Sons.

Several methods have been used to identify structural variability in push-pull conjugated polymers. For some systems, UV-Vis absorption spectroscopy can indicate the presence of homocoupling through a shift in absorption onset. However, this approach does not offer conclusive evidence within a single sample and can only give an indication relative to another sample.[21, 24, 26, 27] Characterization of both end-groups and the occurrence of homocoupling can be done using ^{1}H-NMR spectroscopy for some polymer systems.[25, 26, 28, 29] However, when performed on reasonably high molar mass polymers, the NMR peaks of interest suffer from low signal intensity compared to the polymeric backbone, complicating analysis. Furthermore, systems that tend to aggregate in solution (as often desired for applications) or are limited in solubility cannot properly be analyzed using NMR. In this work, we therefore turn to matrix-assisted laser desorption/ionization time-of-flight (MALDI–ToF) mass spectrometry (MS) as a powerful tool to elucidate on the presence of structural defects.[19, 30] End-group analysis can be done easily by identifying the repeating units and calculating a residual mass, which is then fitted to plausible end-groups. Furthermore, previous MALDI–ToF MS work in our group has confirmed the occurrence of homocoupled defects even at very short reaction times (through a flow polymerization) suggesting that, unlike termination, homocoupling occurs independent of reaction time and is equally likely to be identified in short and long polymer chains.[9] MALDI–ToF MS does, however, suffer from its own set of limitations, since the ionization tendency of varying species can be quite different and no absolute quantification is possible. Somewhat surprisingly, none of these techniques has been applied to donor-acceptor copolymers PM6 and D18 used to prepare state-of-the-art organic solar cells. In fact, very little is known on possible structural defects in these polymers and their possible effect on device performance.

Last year, commercially available Buchwald P(*t*Bu)$_3$ Pd G3 (Figure S1) was used as a pre-catalyst to demonstrate the viability of room-temperature Stille polycondensation to yield conjugated polymers.[31, 32] Furthermore, small molecule model systems were used to screen for the occurrence of homocoupling with different catalysts and temperatures. When reacted at room temperature using P(*t*Bu)$_3$ Pd G3, these small molecules and selected polymers displayed no homocoupled defects. However, when synthesized at higher temperatures or using common catalysts such as Pd_2dba_3/P(*o*-tol)$_3$ and $Pd(PPh_3)_4$, homocoupling was observed. Surprisingly, this Buchwald G3 catalyst was not yet used to synthesize top-performing push-pull polymers for organic solar cells. Polymers such as PM6 and D18, which are synthesized using Pd_2dba_3 / P(*o*-tol)$_3$ and $Pd(PPh_3)_4$, achieve power conversion efficiencies (PCEs) up to 18% in single-junction binary solar cells in combination with non-fullerene acceptors.[33, 34]

Therefore, in the present work, we investigate the possibility to synthesize the state-of-the-art donor-acceptor OPV polymers PM6 and D18 using the Buchwald P(*t*Bu)$_3$ Pd G3 precatalyst at varying temperatures through classical in-flask as well as continuous flow methods, with additional benefits toward upscaling and commercialization.[9] A thorough analysis of the resulting polymer structure, possible defects, and varying end-groups is conducted by MALDI–ToF MS. The effects of the observed structural variability are further analyzed in OPV devices, by using UV-Vis absorption spectroscopy, and by grazing incidence wide-angle X-ray scattering (GIWAXS). Our study highlights the efficacy of P(*t*Bu)$_3$ Pd G3 as a catalyst for the synthesis of PM6 and D18 with minimal structural defects. Although we observed differences in the aggregation behavior of defect-containing and homocoupling-free PM6, the use of this catalyst resulted in polymers that performed comparably to conventionally synthesized ones in organic solar cells. Moreover, the development of a reproducible synthesis protocol (using the Buchwald catalyst) through droplet-flow chemistry is a promising advancement toward reproducible donor-acceptor conjugated polymers for commercial applications.

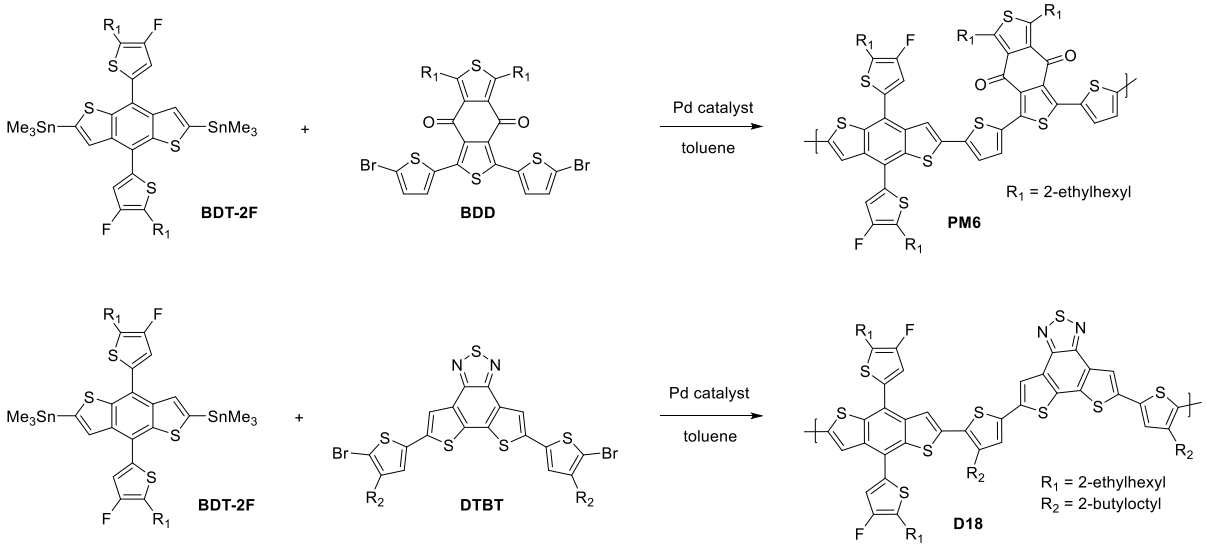

Scheme 1: General polymerization scheme for PM6 and D18 using the Stille cross-coupling.

Results and discussion

PM6 (Scheme 1) was synthesized using three different catalytic systems (Table 1). Detailed synthesis conditions are reported in the Supporting Information. First, **PM6-tetr** was prepared with (fresh) tetrakis according to a literature procedure.[35] Additionally, **PM6-dba-A** and **PM6-dba-B** were obtained using Pd_2dba_3 with P(*o*-tol)$_3$, yielding polymers with slightly higher molar mass, as determined by gel permeation chromatography (GPC) at high temperature (160 °C in trichlorobenzene) to minimize aggregation effects. For **PM6-dba-A,** a fresh bottle of Pd_2dba_3 was used. The Pd_2dba_3 used for **PM6-dba-B** came from a bottle which was open for over a month, although being stored under inert atmosphere in a freezer. By changing the catalyst system to P(*t*Bu)$_3$ Pd G3 and performing the synthesis at room temperature, **PM6-G3-RT** was obtained, with a relatively low molar mass.[32] To achieve a higher molar mass, the synthesis was repeated at elevated temperatures, yielding **PM6-G3-50** and **PM6-G3-100** for reactions at 50 and 100 °C, respectively. All obtained polymers were treated with a scavenging agent (to remove residual palladium traces), subjected to Soxhlet extractions, and precipitated from the chloroform fraction. From **PM6-G3-100**, a chloroform and chlorobenzene fraction (with higher yield; Table S2) were recovered from the Soxhlet extraction. The chloroform fraction showed noticeably lower solubility (in chloroform) compared to the other batches. ^{1}H-NMR spectroscopy analysis was attempted on a polymer sample (**PM6-dba-A**) using either *o*-dichlorobenzene or a solvent mixture of deuterated chloroform and CS_2 (Figure S2). These conditions were selected to reduce the aggregation of the polymer. However, even with these precautions, the obtained spectra were poorly resolved and not suitable for meaningful structural analysis. Electrochemical characterization was performed on all batches through cyclic voltammetry (CV). No significant differences were observed for the highest occupied molecular orbital (HOMO) and lowest unoccupied molecular orbital (LUMO) energies between the different batches (Table S3, Figure S3).

Table 1: Synthesis conditions and molar mass data for all PM6 batches (chloroform fractions).

	Catalyst	Ligand / additive	Temperature (°C)	M_n (kg/mol)	M_w (kg/mol)	$Đ$
PM6-tetr	$Pd(PPh_3)_4$	/	100	29.6	57.0	1.9
PM6-dba-A	Pd_2dba_3	P(*o*-tol)$_3$	100	36.6	70.6	1.9
PM6-dba-B	Pd_2dba_3	P(*o*-tol)$_3$	100	40.3	88.6	2.2
PM6-G3-RT	P(*t*Bu)$_3$Pd G3	K_3PO_4	RT	23.3	44.4	1.9
PM6-G3-50	P(*t*Bu)$_3$Pd G3	K_3PO_4	50	29.0	58.4	2.0
PM6-G3-100	P(*t*Bu)$_3$Pd G3	K_3PO_4	100	28.9	66.5	2.3

All polymer batches were then analyzed by MALDI–ToF MS to investigate how the different catalytic systems affect the chemical structure. In MALDI–ToF MS, the ionization process is competitive. As a result, the observed masses are skewed toward the lower range. It is difficult to determine the extent of this masking because GPC relies on polystyrene standards, which tends to overestimate the actual molar masses of conjugated polymers.[36, 37] Due to the small difference in exact mass between the incorporated BDT-2F and BDD monomers (Scheme 1) of only 6 Da, homocoupling in PM6 results in artificial peak broadening. Therefore, it is needed to elucidate the possible end-groups to distinguish homocoupling from a differently terminated chain. A summary of the analysis is given in Table 2.

The MALDI–ToF mass spectrum of **PM6-tetr** (Figure S4) mainly shows methyl end-groups, with some bromine and hydrogen, suggesting that the main termination pathway is destannylation and methyl transfer.[38] However, these end-groups cannot explain the corresponding peak distributions completely since the theoretical isotopic envelopes of the polymer chains in question only account for a part of the experimental signals. Considering this, extending the fit to chains with an extra donor-donor homocoupling results in a much better match. This is illustrated by the highlighted predicted isotopic

patterns in Figure 2. The calculated pattern of a chain containing 4 BDT-2F (D) and 4 BDD (A) units (hereafter referred to as a D4A4 chain) and two methyl end-groups (*m/z* = 4903.5) constitutes only part of the observed experimental signal, and a quite prominent 'second' overlapping distribution can be distinguished. This signal cannot be fitted to the same D4A4 chain as the next plausible end-group combination after [Me, Me] would be [Ph, H], with the phenyl group being an artifact caused by ligand exchange from tetrakis. The residual mass of these groups (78.1 Da) would result in a monoisotopic signal of this chain at *m/z* = 4951.6, which is too high. Therefore, this overlapping distribution has to be the result of some other combination of a total of 8 BDT-2F and BDD monomers. As illustrated in red, the calculated spectrum of a chain with at least one donor-donor homocoupling, D5A3 [Me, Me] (*m/z* = 4903.5), fits within this region and nicely complements the D4A4 [Me, Me] prediction. This analysis can be repeated in the [Br, Me] terminated region to yield the same conclusion. For homocoupling of the acceptor units, no clear conclusions can be made here. Due to the absence of purely hydrogen end-capped chains, no distinction between homocoupled species and 'ideal' chains with [Me, H] end-groups is possible.

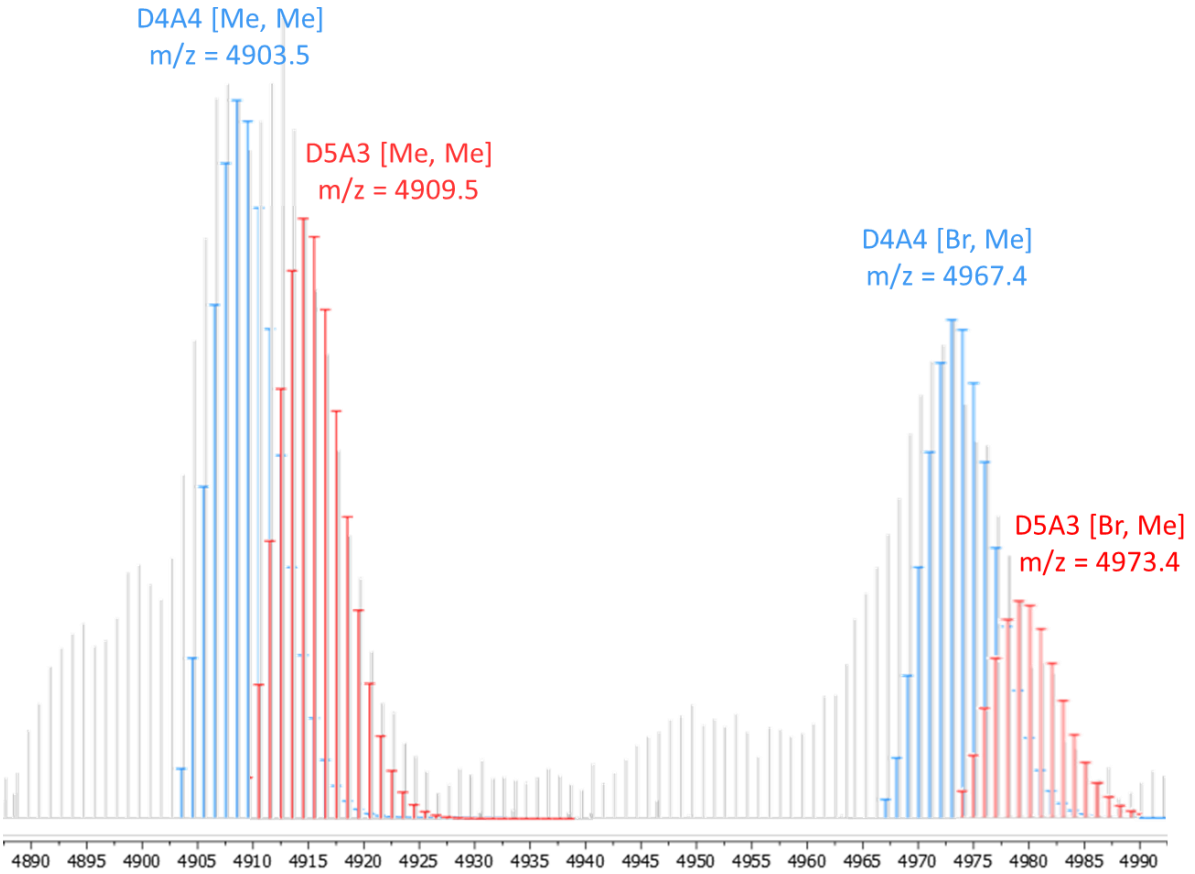

Figure 2: MALDI–ToF mass spectrum excerpt for **PM6-tetr**. Blue: Calculated overlay for D4A4 [Me, Me] (*m/z* = 4903.5) and D4A4 [Br, Me] (*m/z* = 4967.4); Red: Calculated overlay for D5A3 [Me, Me] (*m/z* = 4909.5) and D5A3 [Br, Me] (*m/z* = 4973.4).

Because of the high relative intensity of the D5A3 chain compared to the 'ideal' D4A4 chain, we conclude **PM6-tetr** to have a relatively 'medium' amount of (predominantly BDT-2F) homocoupled defects in the polymeric backbone. We should not forget though that MALDI–ToF MS is not to be treated as a quantitative method and certain species can be over- or under-presented in the spectra. Since a charge-transfer matrix was applied, the electron density of the different species present plays a role as well. Furthermore, one can note that the mass spectrum is in general quite 'dirty', as additional signals are observed in regions that have no fit with the most plausible structures. For

example, past the now identified D5A3 [Me, Me] (*m/z* = 4909.5) distribution, no signal is expected until the monoisotopic signal of the D4A4 [Ph, H] (*m/z* = 4951.5) chain. As can be seen in Figure 2, some signals of unknown origin do appear throughout this region.

PM6-dba-A (Figures S5-6) shows clear differences compared to **PM6-tetr**. Polymer chains are almost exclusively terminated with hydrogen. Apart from hydrogen, a seemingly low amount of methyl, bromine, and trimethylstannyl end-groups can be found in the spectrum. Once again, fitting the calculated isotopic pattern of a single species cannot explain the encountered experimental signals. As illustrated in Figure S6, an acceptor-acceptor homocoupled chain D3A5 [H, H] (*m/z* = 4869.4) is needed to complement the 'ideal' D4A4 [H, H] (*m/z* = 4875.4). Due to the excellent resolution of the spectrum in the D4A4 [Me, H] (*m/z* = 4889.4) region, some BDT-2F homocoupling is observed as well as the signal corresponding to D5A3 [Me, H] (*m/z* = 4895.4). However, since both the BDD and BDT-2F homocoupled chains are relatively low in intensity compared to the 'ideal' D4A4 [H, H] signal, we can conclude that **PM6-dba-A** has a relatively 'low' amount of homocoupled defects in the polymeric structure. End-group-wise, **PM6-dba-B** (Figures S7-8) shows many similarities with **PM6-dba-A**, apart from the presence of more methyl end-groups. A 'medium' amount of acceptor-acceptor homocoupling can be distinguished as a shoulder on the 'ideal' D4A4 [H, H] isotopic pattern (Figure S8). When taking a closer look at the [Me, Me] region, a prominent D5A3 [Me, Me] (*m/z* = 4909.5) signal explains the maximal signal at best, along with higher degrees of donor-donor homocoupling. Therefore, **PM6-dba-B** is proposed to have a relatively 'high' amount of homocoupled defects. This can likely be attributed to the older catalyst used in this case.

The discovery of structural defects in this top-performing polymer led us to question the occurrence of homocoupling in commercial PM6, widely used by scientists active in the OPV field. To this end, two samples of common commercial suppliers were analyzed. For supplier A (Figures S9-10), the PM6 chains are mainly terminated with methyl groups and bromine or phenyl, while some hydrogen is also observed. Interestingly, no distributions correlating to [H, H] end-groups are observed, suggesting a similar synthesis method as **PM6-tetr**. However, several distributions with chlorine are encountered (e.g. at *m/z* = 4923.4, which shows a good fit with [Cl, Me], and [Cl, Br] at *m/z* = 4987.3), which were not seen so far in other samples and which have an unknown origin. Homocoupling-wise (Figure S10), a substantial amount of D5A3 [Me, Me] (*m/z* = 4909.5) signal is observed, similar again to **PM6-tetr**. As a sidenote, the D5A3 [Me, Me] (*m/z* = 4909.5) might be convoluted with signal originating from possibly D5A3 [Cl, H] (4909.4), but since this mass spectrum shows little hydrogen end-groups in other distributions, this contribution is expected to be small. For supplier B (Figures S11-12), many similarities with **PM6-dba-A**/**B** are observed. The polymer is mainly hydrogen end-capped, along with some methyl and a substantial amount of bromine or phenyl. Acceptor homocoupling (Figure S12) is observed as D3A5 [H, H] (*m/z* = 4869.4) and donor homocoupling as D5A3 [Me, Me] (*m/z* = 4909.5). The relative amount is somewhere in between **PM6-dba-A** and **PM6-dba-B**.

When using the Buchwald precatalyst at room temperature, the mass spectrum (Figures S13-14) gets considerably simpler. **PM6-G3-RT** chains containing an extra BDD acceptor monomer have nearly exclusively bromine end-groups. Chains containing equal amounts of BDT-2F and BDD units are terminated with bromine and either a methyl group or an end group so far unencountered with a residual mass of 168.08 Da ($C_{12}H_{10}N$). This mass fits a carbazole-like species (CbzH) that could be originating from the P(*t*Bu)$_3$ Pd G3 catalyst through ligand exchange (Figure S1). A detailed investigation into this end-group's origin is beyond the scope of this study. The predicted isotopic patterns fit the experimental ones nicely, and as a result, no significant homocoupling is observed in **PM6-G3-RT** (Figure S14). **PM6-G3-50** (Figures S15-16) shows more terminated chains compared to **PM6-G3-RT**. Termination mainly occurs via the CbzH pathway described above, in addition to

destannylation. Nonetheless, no significant homocoupling is observed (Figure S16). The spectrum of the chloroform fraction of **PM6-G3-100** (Figures S17-18) shows most chains terminated with CbzH and methyl end-groups. No bromine end-groups are observed. Once again, no significant homocoupling seems to be present in the sample (Figure S18). The species observed in the mass spectrum of the chlorobenzene fraction (Figure S19) are very similar to those in the chloroform fraction.

Summarizing these findings (Table 2), in particular the identification of homocoupling in all batches synthesized with conventional catalysts and in both commercial samples, leads us to conclude that the occurrence of homocoupling in PM6 should be taken as the norm rather than the exception. However, quantification is difficult and there might be considerably less homocoupling than suggested by MALDI–ToF MS.

Table 2: Overview of the MALDI–ToF MS end-group and homocoupling analysis for all PM6 batches.

	Main end-groups	Other end-groups present	Relative amount of homocoupling
PM6-tetr	Me	Br, H	Medium
PM6-dba-A	H	Me, Br, $SnMe_3$	Low
PM6-dba-B	H	Me, Br, $SnMe_3$	High
PM6-G3-RT	Me, Br	CbzH, H	None
PM6-G3-50	CbzH, Me, Br	H	None
PM6-G3-100	CbzH, Me	H	None
Supplier A	Me, Br	H, Cl	Medium
Supplier B	H, Br	Me	Medium

When examining the UV-Vis absorption spectra of the synthesized PM6 batches dissolved in chlorobenzene at room temperature, two distinctive absorption peaks at approximately 615 and 575 nm (Figure 3a) are observed. These peaks correspond to the vibronic 0-0 and 0-1 transitions, respectively, and can be attributed to the distinct molecular aggregation present in PBDB-T and its halogenated derivatives PBDB-T-2F (PM6) and PBDB-T-2Cl, even in solution.[39-42] The ratio of the intensities of these peaks ($I_{0\text{-}0}/I_{0\text{-}1}$) is commonly used in the literature as an indicator of the extent of aggregation and attributed to high molar masses.[6] However, it should be noted that the presence of vibronic features in the absorption spectra indicates the presence of photophysical aggregates, while the ratio of vibronic peaks gives information on the type of aggregates present. A more subtle and broad contribution of the disordered phase centered at 550 nm completes the absorption spectrum at room temperature of neat PM6, which becomes prevalent upon heating.[43] A $I_{0\text{-}0}/I_{0\text{-}1}$ ratio less than unity indicates predominantly H-like aggregates which exhibit interchain exciton coupling, while J-like aggregates with greater intrachain ordering afford a $I_{0\text{-}0}/I_{0\text{-}1}$ ratio greater than unity. Thus, this ratio serves as a helpful marker for along-chain ordering of the polymer. The highest $I_{0\text{-}0}/I_{0\text{-}1}$ ratios are observed in the samples with little to no homocoupling, whereas the absorption spectra for materials with more homocoupling defects (**PM6-tetr** and **PM6-dba-B**) appear quite similar, with lower $I_{0\text{-}0}/I_{0\text{-}1}$ ratios (i.e. reduced intrachain ordering). By heating the solution, the aggregate absorption features decrease in intensity and become more H-like (Table S4, Figure S20-22. However, it is important to acknowledge that a decrease in the presence of disordered chains could also contribute to the apparent reduction in $I_{0\text{-}1}$ and play a part in the observed increase in $I_{0\text{-}0}/I_{0\text{-}1}$ ratio of the less homocoupled samples. To address this, we recorded absolute absorption spectra of both **PM6-tetr** and **PM6-G3-RT** at identical concentrations (see Figure S21b). In these spectra, a clear shift in the vibronic features is evident, whereas the section dominated by disordered absorption (from 460 to 520 nm)[43] shows minimal alteration. This suggests that significant differences in the contribution of disordered chains to the vibronic features are unlikely among the various samples reported here.

When cast into thin films, the absorption spectra of the materials show a similar trend to the solution absorption where the materials with the greatest degree of homocoupling exhibit a lower $I_{0\text{-}0}/I_{0\text{-}1}$ ratio (Figure 3b and 3c). Indeed, while the aggregates in all materials appear strongly J-like, the homocoupling-free materials possess larger $I_{0\text{-}0}/I_{0\text{-}1}$ ratios, characteristic of more planar chains.[44-47] One has to note that these results are in contrast to the reported literature, as $I_{0\text{-}0}/I_{0\text{-}1}$ ratios are typically linked to molar mass rather than homocoupling. Given that hole transport in polymeric semiconductors is very sensitive to intrachain ordering, it is expected that the differences in aggregation behavior may have implications for the performance of OPV devices.

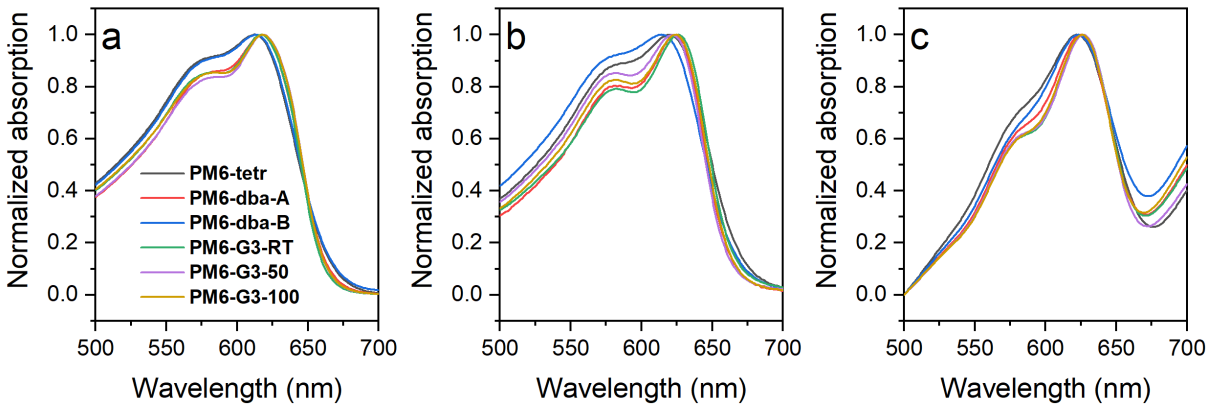

Figure 3: (a) Normalized UV-Vis absorption plots (500–700 nm region) for all PM6 batches diluted in chlorobenzene at room temperature. (b) Normalized UV-Vis absorption plots for all neat polymer films. (c) UV-Vis absorption plots normalized for the PM6 peak for all blend (PM6:Y6, 1:1.2) thin films.

Solar cells were then fabricated from each PM6 batch and the performance parameters are summarized in Table 3. The PM6 samples were blended with the non-fullerene acceptor Y6 (1:1.2 ratio) in chloroform and used as approximately 100 nm thick active layers in devices with an architecture ITO/PEDOT:PSS/active layer/PDIN/Ag. All batches resulted in solar cells (Figure S23) with excellent short-circuit current densities (J_{sc}) above 25 mA/cm². Differences in the open-circuit voltage (V_{oc}) are observed, with **PM6-G3-100** in particular showing a lower V_{oc}. This is somewhat surprising as no large differences in frontier molecular orbital energy levels were found by CV. The main difference between the samples is the fill factor (FF), which does result in significant differences in the overall efficiency. The highest PCE is achieved with **PM6-dba-A**, made using fresh Pd_2dba_3 and in which a low amount of homocoupling was observed. Homocoupling-free **PM6-G3-RT** gives on average a rivaling performance, indicating that low amounts of homocoupling do not have a detrimental impact on the device performance for PM6.

Table 3: Solar cell performance parameters for the devices based on the PM6 batches.

	J_{sc} (mA/cm²)	V_{oc} (V)	FF (%)	PCE (%) (best)
PM6-tetr	25.3 ± 0.4	0.868 ± 0.003	70.7 ± 0.3	15.6 ± 0.2 (15.9)
PM6-dba-A	26.1 ± 0.4	0.854 ± 0.002	73.1 ± 0.4	16.3 ± 0.2 (16.7)
PM6-dba-B	26.0 ± 0.3	0.856 ± 0.002	65.1 ± 0.8	14.5 ± 0.3 (14.8)
PM6-G3-RT	25.8 ± 0.3	0.851 ± 0.001	72.6 ± 0.4	15.9 ± 0.1 (16.1)
PM6-G3-50	25.7 ± 0.5	0.842 ± 0.003	71.3 ± 0.7	15.4 ± 0.2 (15.7)
PM6-G3-100	26.2 ± 0.6	0.834 ± 0.001	60.2 ± 0.6	13.2 ± 0.3 (13.6)

A polymer's molar mass and dispersity are often attributed a key role in the resulting bulk heterojunction blend morphology and device properties.[6, 8, 48] All polymer batches resulted in a decent weight-average molar mass (M_W) of at least 44 kg/mol (Table 1), meaning expected differences in

optoelectronic properties would be small.[8] **PM6-dba-B** and **PM6-G3-100** stand out with a relatively low FF (< 70%). For **PM6-dba-B**, the highest amount of homocoupling and low $I_{0\text{-}0}/I_{0\text{-}1}$ values were identified, despite the high molar mass. The low FF is therefore hypothesized to be caused by a lower amount of polymer aggregation in the blend. For **PM6-G3-100**, the inferior performance is tentatively attributed to the low solubility of this sample, complicating proper film formation.

To investigate the influence of homocoupling on the morphology of the active layer, grazing-incidence wide-angle X-ray scattering (GIWAXS) analysis was performed on blends consisting of **PM6-tetr**, **PM6-dba-B**, or **PM6-G3-RT** with Y6 (Figure 4). The lineouts (Figure 4d) for **PM6-tetr** and **PM6-dba-B** are comparable to reported literature, with the blends exhibiting predominantly face-on texturing.[49] Homocoupling-free **PM6-G3-RT**, on the other hand, shows some structural differences compared to its homocoupled analogues. The texturing of this blend appears more isotropic, with an edge-on population of crystallites present. These edge-on crystallites are expected to be from the PM6 phase as Y6 is typically face-on.[50] Most notably, an in-plane peak at Q_{xy} = 0.65 Å^{-1}, attributed to a PM6 backbone reflection, appears much more prominent in the homocoupling-free material. The increased prominence of this backbone reflection in the homocoupling-free material is consistent with greater chain-to-chain registry in the crystallites as one would expect from elimination of such structural defects.

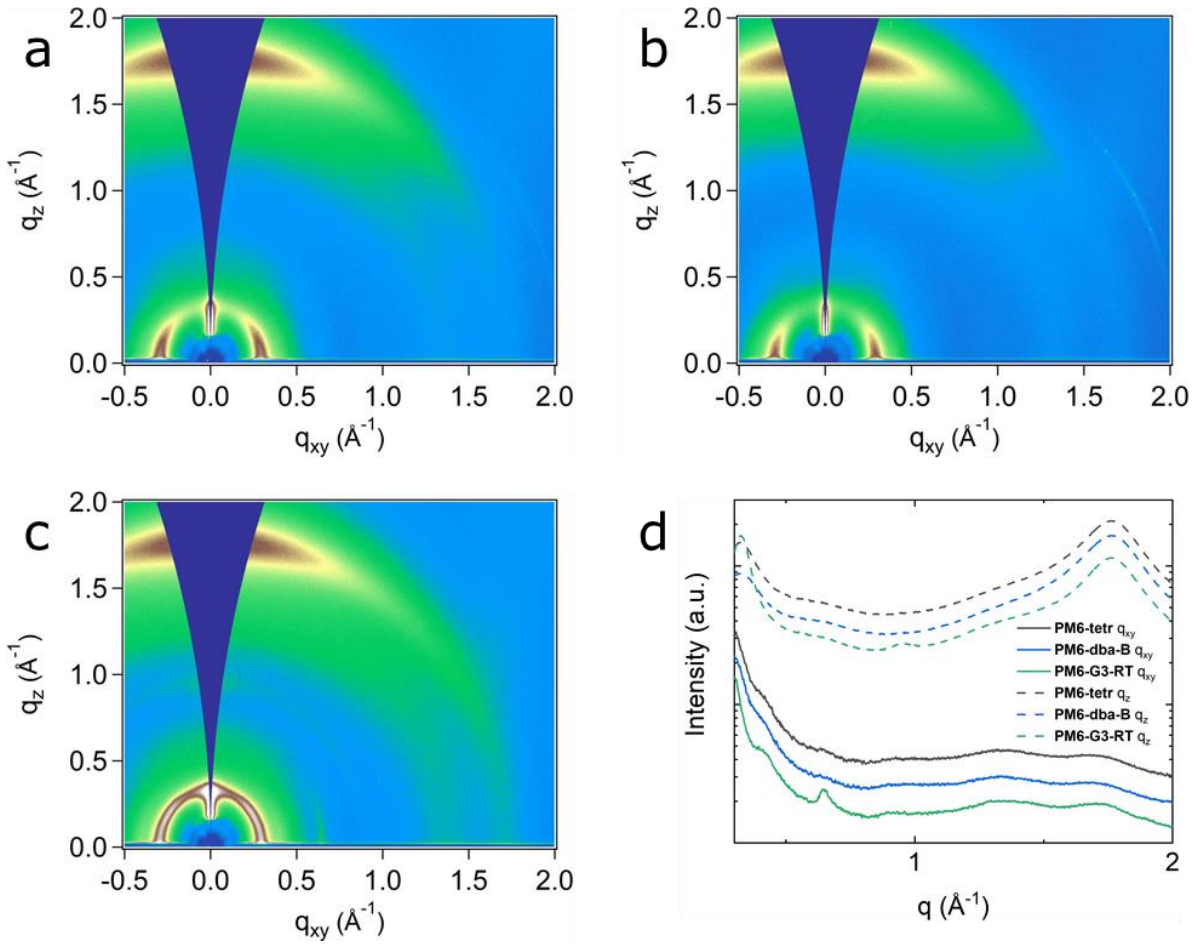

Figure 4: Two-dimensional GIWAXS patterns for films of PM6:Y6 (1:1.2) based on (a) **PM6-tetr**, (b) **PM6-dba-B**, and (c) **PM6-G3-RT** (b). (d) GIWAXS lineplots for PM6:Y6 blends based on **PM6-tetr**, **PM6-dba-B**, and **PM6-G3-RT** (offset for clarity). All films were thermally annealed at 100 °C for 10 minutes.

To verify for a second relevant polymer if the application of the room-temperature G3 catalyst is beneficial, D18 was synthesized using the same catalytic systems as applied for PM6 (Table 4). No homocoupling was observed in any of the commercial samples or synthesized batches, except when utilizing the P(*t*Bu)$_3$ Pd G3 catalyst at 100 °C (Table S8). Due to the low intensity of the signal and the absence of signals corresponding to multiply homocoupled chains, the estimated amount of homocoupling in this sample is (very) low. The $I_{0\text{-}0}/I_{0\text{-}1}$ ratio and device performance follow the trend of the molar mass. D18 synthesized by Pd_2dba_3 and P(*t*Bu)$_3$ Pd G3 at 100 °C both resulted in highly efficient devices with PCEs around 17% (Table 5). Overall, the D18 system seems less prone to homocoupling and benefits solely from achieving an optimal molar mass. A more detailed discussion on the analysis of the D18 samples can be found in the Supporting Information.

Table 4: Synthesis conditions and molar mass data for all D18 batches (chloroform fractions).

	Catalyst	Ligand / additive	Temperature (°C)	M_n (kg/mol)	M_w (kg/mol)	$Đ$
D18-tetr	$Pd(PPh_3)_4$	/	100	11.2	19.2	1.7
D18-dba	Pd_2dba_3	P(*o*-tol)$_3$	100	36.6	84.2	2.3
D18-RT	P(*t*Bu)$_3$Pd G3	K_3PO_4	25	27.6	43.3	1.6
D18-50	P(*t*Bu)$_3$Pd G3	K_3PO_4	50	31.6	59.5	1.9
D18-100	P(*t*Bu)$_3$Pd G3	K_3PO_4	100	38.2	72.1	1.9

Table 5: Solar cell performance parameters for the solar cell devices based on the D18 batches.

	J_{sc} (mA/cm²)	V_{oc} (V)	FF (%)	PCE (%) (best)
D18-dba	26.6 ± 0.4	0.876 ± 0.002	72.0 ± 0.5	16.8 ± 0.3 (17.2)
D18-G3-RT	22.3 ± 0.5	0.837 ± 0.002	59.0 ± 1.0	11.0 ± 0.1 (11.2)
D18-G3-50	24.4 ± 0.5	0.864 ± 0.003	70.6 ± 0.3	14.9 ± 0.4 (15.4)
D18-G3-100	26.1 ± 0.3	0.866 ± 0.002	75.0 ± 0.5	17.0 ± 0.3 (17.4)

Finally, in order to increase reproducibility and allow for easy scale-up, the synthesis using P(*t*Bu)$_3$ Pd G3 was translated to a droplet-flow protocol.[9] PM6 was selected for this purpose due to the larger variations encountered in the structures of in-flask prepared and commercial PM6 batches. Since a homogeneous reaction mixture is required to prevent clogging of the reactor tubing and K_3PO_4 shows poor solubility in toluene, the more soluble bases pyridine, NaO*t*Bu, and KO*t*Bu were first investigated in a standard in-flask synthesis. To push the reaction to completion, the polymerization was performed overnight and at an elevated temperature of 100 °C. The results are summarized in Table S10. None of the base replacement candidates showed promise in in-flask polymerizations, so instead a saturated solution of K_3PO_4 in toluene was used for the following flow experiments. The detailed flow procedure used can be found in the Supporting Information. In order to screen for an optimal reaction temperature and residence time, several plugs of 0.1 mL reaction mixture were injected into the flow reactor (Figure S36) and propelled through with perfluoropolyether (PFPE) at various flow rates and temperatures, after which the polymer samples were collected by precipitation in methanol and analyzed using GPC (Figure 5, Table S11). MALDI–ToF MS analysis showed no signs of homocoupling in any of the samples.

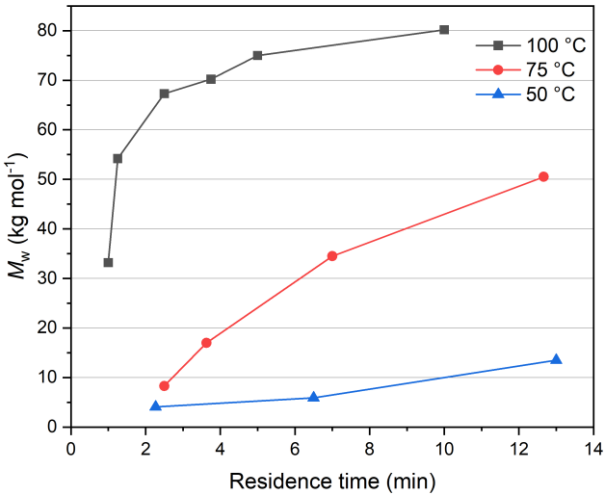

Figure 5: Molar mass plot for the PM6 synthesis using plug flow at different residence times and temperatures.

At room temperature, no significant polymerization occurred, even after a residence time of 30 minutes. In order to prevent the clogging of the reactor tubing before the PFPE mixing T-piece, the reaction temperature was increased rather than further reducing the flow rate. At 50 °C, long residence times are still needed to achieve proper polymerization. At 100 °C, high molar masses, similar to **PM6-G3-100**, were obtained, even after only 2 minutes. Such high molar masses proved detrimental to device performance as solubility decreases (Table 3). Accurately controlling the molar mass through residence time at such fast flow rates is impractical, so the synthesis was performed at 75 °C as a compromise between high molar masses and practical flow rates (Figure 5). These conditions offer excellent molar mass tunability, while keeping the residence time short.

Similar to the in-flask synthesis, all crude polymers were treated with a scavenging agent for residual palladium, precipitated in methanol, and subjected to a Soxhlet extraction. However, to separate the polymers from the fluorinated PFPE carrier liquid, an extraction using low boiling PFPE had to be performed first. All detailed information can be found in the Supporting Information. To investigate the reproducibility of this method, all syntheses were performed in duplo. According to the screening experiment (Figure 5), molar masses of 30, 40, and 50 kg/mol can be targeted by performing the synthesis over residence times of approximately 6, 9, and 12.5 minutes. The synthesis results and electrochemical data are summarized in Table 6, Figure S37, and Table S12. Excellent reproducibility was achieved at each residence time, affording near-identical polymer samples in terms of molar mass and dispersity. All batches gave nearly identical MALDI–ToF mass spectra. They strongly resemble the spectra obtained for **PM6-G3-RT** and **PM6-G3-50** (Figures S38-39).

Table 6: Residence times and molar mass data for all droplet-flow PM6 samples (chloroform fractions).

	Residence time (min)	M_n (kg/mol)	M_w (kg/mol)	$Đ$
Flow-35k-A	6	18.6	35.5	1.9
Flow-35k-B	6	18.9	35.5	1.9
Flow-40k-A	9	21.0	41.2	2.0
Flow-40k-B	9	20.7	40.7	2.0
Flow-50k-A	12.5	24.9	51.3	2.1
Flow-50k-B	12.5	24.9	52.9	2.1

Solar cell devices were then also fabricated with the droplet-flow PM6 samples, using an identical configuration and procedure as for the in-flask PM6 samples (Table7, Figure S40). Cells based on PM6 from **Flow-35k-A** and **Flow-35k-B** have a slightly lower J_{sc} and FF compared to the other materials. Although this is not investigated further, the somewhat lower molar mass could be at play here. Devices based on all other samples perform similar, with PCEs rivaling those achieved for **PM6-G3-RT**. Furthermore, the excellent reproducibility in the synthesis is translated into small variations in performance between the duplo samples.

Table 7: Solar cell performance parameters for the devices based on the droplet-flow based PM6.

	J_{sc} (mA/cm²)	V_{oc} (V)	FF (%)	PCE (%) (best)
Flow-35k-A	24.4 ± 0.4	0.838 ± 0.002	68.1 ± 0.8	14.0 ± 0.2 (14.4)
Flow-35k-B	24.9 ± 0.5	0.837 ± 0.002	67.3 ± 1.3	14.0 ± 0.3 (14.6)
Flow-40k-A	26.2 ± 0.5	0.840 ± 0.002	71.7 ± 0.9	15.8 ± 0.3 (16.3)
Flow-40k-B	25.9 ± 0.7	0.841 ± 0.002	71.8 ± 0.7	15.6 ± 0.4 (16.2)
Flow-50k-A	26.1 ± 0.4	0.835 ± 0.001	71.6 ± 0.8	15.6 ± 0.3 (16.1)
Flow-50k-B	26.1 ± 0.3	0.837 ± 0.002	70.0 ± 0.7	15.3 ± 0.3 (15.9)

Conclusions

The presence of homocoupling was identified in the top-performing OPV donor polymer PM6, both in commercial and self-made samples synthesized with conventional catalysts, using MALDI–ToF mass spectrometry. Subsequently, homocoupling-free PM6 was prepared at room temperature, demonstrating comparable photovoltaic performance to batches made with the conventional catalysts at high temperature, despite having a significantly lower molar mass. Increasing the molar mass through the use of higher polymerization temperatures did not result in improved solar cell efficiencies. A correlation between the amount of homocoupling in PM6 and the type of aggregation was observed, as less homocoupling seems to induce more J-like aggregation with greater intrachain ordering. The interplay between molar mass and the exact polymer structure (homocoupling and varying end-groups) determines the performance of these materials in photovoltaic devices. For D18, no homocoupling was found in commercial samples or when made with Pd_2dba_3. Using P(*t*Bu)$_3$ Pd G3, homocoupling was identified when performing the polymerization at elevated temperature. The (estimated) low amount of homocoupling resulting from these conditions does not seem to affect the device performance, while an increased molar mass benefits the efficiency. Overall, the comparison between PM6 and D18, polymers with close structural resemblance, indicates that the occurrence of homocoupling and the effects of its elimination are system dependent. Finally, a reproducible droplet-flow protocol was established for the synthesis of homocoupling-free PM6 with targeted molar mass. We believe such a protocol can be used for the reproducible synthesis of high-performance conjugated polymers with minimal batch-to-batch variability, providing a stimulus for commercial uptake of these materials and the resulting optoelectronic devices.

Supporting information

Additional information on the PM6 synthesis, characterization, device fabrication, and GIWAXS analysis can be found in the Supporting Information document, alongside a more detailed discussion on the D18 results and the droplet flow procedure.

Acknowledgements

The UHasselt co-authors acknowledge financial support from Hasselt University (BOF incentive funds 19INC10MAE and 19INC12MAE), the Research Foundation – Flanders (FWO Vlaanderen; Ph.D. fellowships S.S. and J.V., projects V413722N, G0D0118N, G0B2718N, GOH3816NAUHL, and I006320N),

the European Union's Horizon 2020 research and innovation program under the Marie-Curie grant (agreement no 882794), and the European Research Council (ERC, grant agreement 864625). T.J.Q. acknowledges support from the National Science Foundation Graduate Research Fellowship Program under grant DGE-1656518. This material is based upon work supported by the U.S. Department of Energy, Office of Science, Office of Workforce Development for Teachers and Scientists, Office of Science Graduate Student Research (SCGSR) program. The SCGSR program is administered by the Oak Ridge Institute for Science and Education for the DOE under contract number DE-SC0014664. Use of the Stanford Synchrotron Radiation Light source, SLAC National Accelerator Laboratory, is supported by the U.S. Department of Energy, Office of Science, Office of Basic Energy Sciences under Contract No. DE-AC02-76SF00515. Part of this work was performed at the Stanford Nano Shared Facilities (SNSF), supported by the National Science Foundation under award ECCS-2026822. The authors thank Prof. Alberto Salleo for his support and Christina Cheng for discussions on the GIWAXS analysis.

References

(1) Zhang, G.; Lin, F. R.; Qi, F.; Heumuller, T.; Distler, A.; Egelhaaf, H. J.; Li, N.; Chow, P. C. Y.; Brabec, C. J.; Jen, A. K.; et al. Renewed Prospects for Organic Photovoltaics. *Chem. Rev.* **2022**, *122* (18), 14180-14274. DOI: 10.1021/acs.chemrev.1c00955.

(2) Ren, H.; Chen, J. D.; Li, Y. Q.; Tang, J. X. Recent Progress in Organic Photodetectors and their Applications. *Adv. Sci.* **2020**, *8* (1), 2002418. DOI: 10.1002/advs.202002418.

(3) Rivnay, J.; Inal, S.; Salleo, A.; Owens, R. M.; Berggren, M.; Malliaras, G. G. Organic Electrochemical Transistors. *Nat. Rev. Mater.* **2018**, *3* (2), 17086. DOI: 10.1038/natrevmats.2017.86.

(4) Zhang, L.; Jia, T.; Pan, L.; Wu, B.; Wang, Z.; Gao, K.; Liu, F.; Duan, C.; Huang, F.; Cao, Y. 15.4% Efficiency All-Polymer Solar Cells. *Sci. China Chem.* **2021**, *64* (3), 408-412. DOI: 10.1007/s11426-020-9935-2.

(5) Helgesen, M.; Carlé, J. E.; dos Reis Benatto, G. A.; Søndergaard, R. R.; Jørgensen, M.; Bundgaard, E.; Krebs, F. C. Making Ends Meet: Flow Synthesis as the Answer to Reproducible High-Performance Conjugated Polymers on the Scale that Roll-to-Roll Processing Demands. *Adv. Energy Mater.* **2015**, *5* (9), 1401996. DOI: 10.1002/aenm.201401996.

(6) Liu, Q.; Fang, J.; Wu, J.; Zhu, L.; Guo, X.; Liu, F.; Zhang, M. Tuning Aggregation Behavior of Polymer Donor via Molecular-Weight Control for Achieving 17.1% Efficiency Inverted Polymer Solar Cells. *Chin. J. Chem.* **2021**, *39* (7), 1941-1947. DOI: https://doi.org/10.1002/cjoc.202100112.

(7) Zhao, T.; Wang, H.; Pu, M.; Lai, H.; Chen, H.; Zhu, Y.; Zheng, N.; He, F. Tuning the Molecular Weight of Chlorine-Substituted Polymer Donors for Small Energy Loss. *Chin. J. Chem.* **2021**, *39* (6), 1651-1658. DOI: 10.1002/cjoc.202000735.

(8) Shi, M.; Wang, T.; Wu, Y.; Sun, R.; Wang, W.; Guo, J.; Wu, Q.; Yang, W.; Min, J. The Intrinsic Role of Molecular Mass and Polydispersity Index in High-Performance Non-Fullerene Polymer Solar Cells. *Adv. Energy Mater.* **2020**, *11* (1), 2002709. DOI: 10.1002/aenm.202002709.

(9) Beckers, O.; Smeets, S.; Lutsen, L.; Maes, W. Perspective on the Application of Continuous Flow Chemistry for Polymer-Based Organic Electronics. *J. Mater. Chem. C* **2022**, *10* (5), 1606-1616. DOI: https://doi.org/10.1039/D1TC04635G.

(10) Bannock, J. H.; Krishnadasan, S. H.; Nightingale, A. M.; Yau, C. P.; Khaw, K.; Burkitt, D.; Halls, J. J. M.; Heeney, M.; de Mello, J. C. Continuous Synthesis of Device-Grade Semiconducting Polymers in Droplet-Based Microreactors. *Adv. Funct. Mater.* **2013**, *23* (17), 2123-2129. DOI: 10.1002/adfm.201203014.

(11) Beckers, O.; Gielen, S.; Verstraeten, F.; Verstappen, P.; Lutsen, L.; Vandewal, K.; Maes, W. Continuous Droplet Flow Synthesis of a Near-Infrared Responsive Push–Pull Copolymer toward Large Scale Implementation of Organic Photodetectors. *ACS Appl. Polym. Mater.* **2020**, *2* (11), 4373-4378. DOI: 10.1021/acsapm.0c00998.

(12) Cordovilla, C.; Bartolomé, C.; Martínez-Ilarduya, J. M.; Espinet, P. The Stille Reaction, 38 Years Later. *ACS Catal.* **2015**, *5* (5), 3040-3053. DOI: 10.1021/acscatal.5b00448.

(13) Leclerc, M.; Brassard, S.; Beaupré, S. Direct (Hetero)Arylation Polymerization: toward Defect-Free Conjugated Polymers. *Polym. J.* **2019**, *52* (1), 13-20. DOI: 10.1038/s41428-019-0245-9.

(14) Chen, H.; He, M.; Pei, J.; Liu, B. End-Group Analysis of Blue Light-Emitting Polymers using Matrix-Assisted Laser Desorption/Ionization Time-of-Flight Mass Spectrometry. *Anal. Chem.* **2002**, *74* (24), 6252-6258. DOI: 10.1021/ac020528h.

(15) Dhanabalan, A.; van Hal, P. A.; van Duren, J. K. J.; van Dongen, J. L. J.; Janssen, R. A. J. Design and Synthesis of Processible Functional Copolymers. *Synth. Met.* **2001**, *119* (1), 169-170. DOI: https://doi.org/10.1016/S0379-6779(00)01316-3.

(16) Dhanabalan, A.; van Dongen, J. L. J.; van Duren, J. K. J.; Janssen, H. M.; van Hal, P. A.; Janssen, R. A. J. Synthesis, Characterization, and Electrooptical Properties of a New Alternating N-dodecylpyrrole-benzothiadiazole Copolymer. *Macromolecules* **2001**, *34* (8), 2495-2501, Article. DOI: 10.1021/ma001732e.

(17) Lo, C. K.; Wolfe, R. M. W.; Reynolds, J. R. From Monomer to Conjugated Polymer: A Perspective on Best Practices for Synthesis. *Chem. Mater.* **2021**, *33* (13), 4842-4852. DOI: 10.1021/acs.chemmater.1c01142.

(18) Vangerven, T.; Verstappen, P.; Drijkoningen, J.; Dierckx, W.; Himmelberger, S.; Salleo, A.; Vanderzande, D.; Maes, W.; Manca, J. V. Molar Mass versus Polymer Solar Cell Performance: Highlighting the Role of Homocouplings. *Chem. Mater.* **2015**, *27* (10), 3726-3732. DOI: 10.1021/acs.chemmater.5b00939.
(19) Pirotte, G.; Verstappen, P.; Vanderzande, D.; Maes, W. On the "True" Structure of Push-Pull-Type Low-Bandgap Polymers for Organic Electronics. *Adv. Electron. Mater.* **2018**, *4* (10), 1700481. DOI: 10.1002/aelm.201700481.
(20) Rudenko, A. E.; Thompson, B. C. Optimization of Direct Arylation Polymerization (DArP) through the Identification and Control of Defects in Polymer Structure. *J. Polym. Sci. A: Polym. Chem.* **2015**, *53* (2), 135-147. DOI: 10.1002/pola.27279.
(21) Hendriks, K. H.; Li, W.; Heintges, G. H. L.; van Pruissen, G. W. P.; Wienk, M. M.; Janssen, R. A. J. Homocoupling Defects in Diketopyrrolopyrrole-Based Copolymers and Their Effect on Photovoltaic Performance. *J. Am. Chem. Soc.* **2014**, *136* (31), 11128-11133. DOI: 10.1021/ja505574a.
(22) Streiter, M.; Beer, D.; Meier, F.; Göhler, C.; Lienert, C.; Lombeck, F.; Sommer, M.; Deibel, C. Homocoupling Defects in a Conjugated Polymer Limit Exciton Diffusion. *Adv. Funct. Mater.* **2019**, *29* (46), 1903936. DOI: 10.1002/adfm.201903936.
(23) Lu, L.; Zheng, T.; Xu, T.; Zhao, D.; Yu, L. Mechanistic Studies of Effect of Dispersity on the Photovoltaic Performance of PTB7 Polymer Solar Cells. *Chem. Mater.* **2015**, *27* (2), 537-543. DOI: 10.1021/cm5042953.
(24) Vangerven, T.; Verstappen, P.; Patil, N.; D'Haen, J.; Cardinaletti, I.; Benduhn, J.; Van den Brande, N.; Defour, M.; Lemaur, V.; Beljonne, D.; et al. Elucidating Batch-to-Batch Variation Caused by Homocoupled Side Products in Solution-Processable Organic Solar Cells. *Chem. Mater.* **2016**, *28* (24), 9088-9098. DOI: 10.1021/acs.chemmater.6b04143.
(25) Lombeck, F.; Komber, H.; Fazzi, D.; Nava, D.; Kuhlmann, J.; Stegerer, D.; Strassel, K.; Brandt, J.; de Zerio Mendaza, A. D.; Müller, C.; et al. On the Effect of Prevalent Carbazole Homocoupling Defects on the Photovoltaic Performance of PCDTBT:$PC_{71}BM$ Solar Cells. *Adv. Energy Mater.* **2016**, *6* (21), 1601232. DOI: 10.1002/aenm.201601232.
(26) Wakioka, M.; Takahashi, R.; Ichihara, N.; Ozawa, F. Mixed-Ligand Approach to Palladium-Catalyzed Direct Arylation Polymerization: Highly Selective Synthesis of π-Conjugated Polymers with Diketopyrrolopyrrole Units. *Macromolecules* **2017**, *50* (3), 927-934. DOI: 10.1021/acs.macromol.6b02679.
(27) Pirotte, G.; Kesters, J.; Cardeynaels, T.; Verstappen, P.; D'Haen, J.; Lutsen, L.; Champagne, B.; Vanderzande, D.; Maes, W. The Impact of Acceptor-Acceptor Homocoupling on the Optoelectronic Properties and Photovoltaic Performance of PDTSQx(ff) Low Bandgap Polymers. *Macromol. Rapid Commun.* **2018**, *39* (14), 1800086. DOI: 10.1002/marc.201800086.
(28) Lombeck, F.; Matsidik, R.; Komber, H.; Sommer, M. Simple Synthesis of P(Cbz-alt-TBT) and PCDTBT by Combining Direct Arylation with Suzuki Polycondensation of Heteroaryl Chlorides. *Macromol. Rapid Commun.* **2015**, *36* (2), 231-237. DOI: 10.1002/marc.201400437.
(29) Broll, S.; Nübling, F.; Luzio, A.; Lentzas, D.; Komber, H.; Caironi, M.; Sommer, M. Defect Analysis of High Electron Mobility Diketopyrrolopyrrole Copolymers Made by Direct Arylation Polycondensation. *Macromolecules* **2015**, *48* (20), 7481-7488. DOI: 10.1021/acs.macromol.5b01843.
(30) Kuwabara, J.; Fujie, Y.; Maruyama, K.; Yasuda, T.; Kanbara, T. Suppression of Homocoupling Side Reactions in Direct Arylation Polycondensation for Producing High Performance OPV Materials. *Macromolecules* **2016**, *49* (24), 9388-9395. DOI: 10.1021/acs.macromol.6b02380.
(31) Bruno, N. C.; Niljianskul, N.; Buchwald, S. L. N-Substituted 2-Aminobiphenylpalladium Methanesulfonate Precatalysts and Their Use in C–C and C–N Cross-Couplings. *J. Org. Chem.* **2014**, *79* (9), 4161-4166. DOI: 10.1021/jo500355k.
(32) Ma, B.; Shi, Q.; Ma, X.; Li, Y.; Chen, H.; Wen, K.; Zhao, R.; Zhang, F.; Lin, Y.; Wang, Z.; et al. Defect-Free Alternating Conjugated Polymers Enabled by Room-Temperature Stille Polymerization. *Angew. Chem. Int. Ed.* **2022**, *61* (16), e202115969. DOI: 10.1002/anie.202115969.

(33) Zhu, L.; Zhang, M.; Xu, J.; Li, C.; Yan, J.; Zhou, G.; Zhong, W.; Hao, T.; Song, J.; Xue, X.; et al. Single-Junction Organic Solar Cells with over 19% Efficiency Enabled by a Refined Double-Fibril Network Morphology. *Nat. Mater.* **2022**, *21* (6), 656-663. DOI: 10.1038/s41563-022-01244-y.
(34) Liu, Q.; Jiang, Y.; Jin, K.; Qin, J.; Xu, J.; Li, W.; Xiong, J.; Liu, J.; Xiao, Z.; Sun, K.; et al. 18% Efficiency Organic Solar Cells. *Sci. Bull.* **2020**, *65* (4), 272-275. DOI: 10.1016/j.scib.2020.01.001.
(35) Zhang, M.; Guo, X.; Ma, W.; Ade, H.; Hou, J. A Large-Bandgap Conjugated Polymer for Versatile Photovoltaic Applications with High Performance. *Adv. Mater.* **2015**, *27* (31), 4655-4660. DOI: 10.1002/adma.201502110.
(36) Gu, K.; Onorato, J.; Xiao, S. S.; Luscombe, C. K.; Loo, Y.-L. Determination of the Molecular Weight of Conjugated Polymers with Diffusion-Ordered NMR Spectroscopy. *Chem. Mater.* **2018**, *30* (3), 570-576. DOI: https://doi.org/10.1021/acs.chemmater.7b05063.
(37) Warr, D. A.; Perdigao, L. M. A.; Pinfold, H.; Blohm, J.; Stringer, D.; Leventis, A.; Bronstein, H.; Troisi, A.; Costantini, G. Sequencing Conjugated Polymers by Eye. *Sci. Adv.* **2018**, *4* (6), eaas9543. DOI: 10.1126/sciadv.aas9543.
(38) Brouwer, F.; Alma, J.; Valkenier, H.; Voortman, T. P.; Hillebrand, J.; Chiechi, R. C.; Hummelen, J. C. Using Bis(pinacolato)diboron to Improve the Quality of Regioregular Conjugated Co-Polymers. *J. Mater. Chem.* **2011**, *21* (5), 1582-1592. DOI: 10.1039/c0jm02359k.
(39) Zhu, D.; Bao, X.; Zhu, Q.; Gu, C.; Qiu, M.; Wen, S.; Wang, J.; Shahid, B.; Yang, R. Thienothiophene-Based Copolymers for High-Performance Solar Cells, Employing Different Orientations of the Thiazole Group as a π Bridge. *Energy Environ. Sci.* **2017**, *10* (2), 614-620, 10.1039/C6EE03186B. DOI: 10.1039/C6EE03186B.
(40) Zheng, Z.; Yao, H.; Ye, L.; Xu, Y.; Zhang, S.; Hou, J. PBDB-T and its Derivatives: A Family of Polymer Donors Enables over 17% Efficiency in Organic Photovoltaics. *Mater. Today* **2019**, *35*, 115-130. DOI: 10.1016/j.mattod.2019.10.023.
(41) Liao, X.; Zhang, L.; Chen, L.; Hu, X.; Ai, Q.; Ma, W.; Chen, Y. Room Temperature Processed Polymers for High-Efficient Polymer Solar Cells with Power Conversion Efficiency over 9%. *Nano Energy* **2017**, *37*, 32-39. DOI: https://doi.org/10.1016/j.nanoen.2017.05.008.
(42) Wang, Q.; Wang, Y.; Zheng, W.; Shahid, B.; Qiu, M.; Wang, D.; Zhu, D.; Yang, R. Regulating Molecular Aggregations of Polymers via Ternary Copolymerization Strategy for Efficient Solar Cells. *ACS Appl. Mater. Interfaces* **2017**, *9* (37), 32126-32134. DOI: 10.1021/acsami.7b09565.
(43) Kroh, D.; Eller, F.; Schötz, K.; Wedler, S.; Perdigón-Toro, L.; Freychet, G.; Wei, Q.; Dörr, M.; Jones, D.; Zou, Y.; et al. Identifying the Signatures of Intermolecular Interactions in Blends of PM6 with Y6 and N4 Using Absorption Spectroscopy. *Adv. Funct. Mater.* **2022**, *32* (44), 2205711. DOI: https://doi.org/10.1002/adfm.202205711.
(44) Chang, X.; Balooch Qarai, M.; Spano, F. C. HJ-Aggregates of Donor-Acceptor-Donor Oligomers and Polymers. *J. Chem. Phys.* **2021**, *155* (3), 034905. DOI: https://doi.org/10.1063/5.0054877.
(45) Clark, J.; Silva, C.; Friend, R. H.; Spano, F. C. Role of Intermolecular Coupling in the Photophysics of Disordered Organic Semiconductors: Aggregate Emission in Regioregular Polythiophene. *Phys. Rev. Lett.* **2007**, *98* (20), 206406. DOI: 10.1103/PhysRevLett.98.206406.
(46) Spano, F. C. Modeling Disorder in Polymer Aggregates: The Optical Spectroscopy of Regioregular Poly(3-hexylthiophene) Thin Films. *J. Chem. Phys.* **2005**, *122* (23), 234701. DOI: https://doi.org/10.1063/1.1914768.
(47) Clark, J.; Chang, J.-F.; Spano, F. C.; Friend, R. H.; Silva, C. Determining Exciton Bandwidth and Film Microstructure in Polythiophene Films Using Linear Absorption Spectroscopy. *Appl. Phys. Lett.* **2009**, *94* (16). DOI: 10.1063/1.3110904.
(48) Liu, Q.; Smeets, S.; Mertens, S.; Xia, Y.; Valencia, A.; D'Haen, J.; Maes, W.; Vandewal, K. Narrow Electroluminescence Linewidths for Reduced Nonradiative Recombination in Organic Solar Cells and Near-Infrared Light-Emitting Diodes. *Joule* **2021**, *5* (9), 2365-2379. DOI: https://doi.org/10.1016/j.joule.2021.06.010.
(49) Zhang, G.; Chen, X. K.; Xiao, J.; Chow, P. C. Y.; Ren, M.; Kupgan, G.; Jiao, X.; Chan, C. C. S.; Du, X.; Xia, R.; et al. Delocalization of Exciton and Electron Wavefunction in Non-Fullerene Acceptor Molecules

Enables Efficient Organic Solar Cells. *Nat. Commun.* **2020**, *11* (1), 3943. DOI: 10.1038/s41467-020-17867-1.
(50) Cheng, C.; Wong, S.; LeCroy, G.; Schneider, S.; Gomez, E.; Toney, M. F.; Salleo, A. Linking Phase Behavior to Performance Parameters in Non-Fullerene Acceptor Solar Cells. *Adv. Energy Mater.* **2023**, *13* (16), 2204297. DOI: 10.1002/aenm.202204297.

TOC graphic

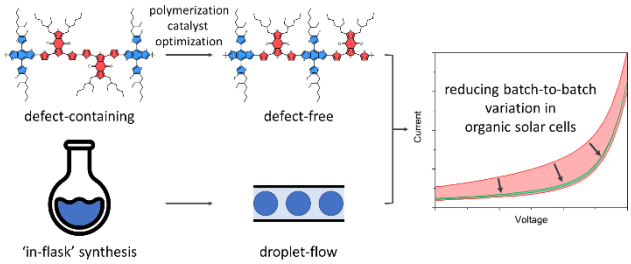
polymerization
catalyst
optimization
defect-containing
defect-free
'in-flask' synthesis
droplet-flow
reducing batch-to-batch
variation in
organic solar cells
Current
Voltage